Optics Letters

Broadband amplitude, frequency, and polarization splitter for terahertz frequencies using parallel-plate waveguide technology

A. I. Hernandez-Serrano,[1] Daniel M. Mittleman,[2] and Emma Pickwell-MacPherson[1,*]

[1]Department of Physics, University of Warwick, Gibbet Hill Road, Coventry, CV4 7AL, UK
[2]School of Engineering, Brown University, Providence, Rhode Island 02912, USA
*Corresponding author: e.macpherson@warwick.ac.uk

Received 7 October 2019; revised 7 November 2019; accepted 17 November 2019; posted 22 November 2019 (Doc. ID 379411); published 25 February 2020

In this Letter, we report a broadband frequency/polarization demultiplexer based on parallel-plate waveguides (PPWGs) for terahertz (THz) frequencies. The fabrication and experimental validation of this polarization sensitive demultiplexer is demonstrated for the range from 0.2 to 1 THz. Upgrading the demultiplexer by adding a second demultiplexer stage, a fifty-fifty amplitude splitter is also demonstrated in the same frequency range. The multiplexer is based on a stainless-steel traveling-wave antenna, exhibiting strong mechanical robustness. This unique device exhibits three splitting mechanisms in the same device: amplitude, polarization, and frequency splitting. This is a significant improvement for the next generation of THz passive components for communication purposes.

https://doi.org/10.1364/OL.45.001208

In recent years, terahertz (THz) radiation has attracted the attention of researchers in the communication area due to the large available bandwidth for wireless signals [1,2]. Tremendous efforts have been made in the study of integrated THz devices for polarization control, demultiplexing/multiplexing, and beam forming, among other applications [3–9]. In the past decade, numerous experiments have proved that THz systems have the capability of transmitting information at rates of tens of gigabits per second or higher [5,10,11–13]. Yet many compelling requirements remain unfulfilled, so the investigation of new devices and components for this frequency range is very important. A key issue for wireless systems is the attenuation of THz signals at specific frequencies by atmospheric water vapor [14–16]. This means that future THz wireless systems will need to operate in certain specific frequency ranges where the intrinsic atmospheric absorption is low.

One essential device for any communication system is a multiplexer/demultiplexer (mux/demux) which is capable of separating a broadband signal into its individual components. Additionally, a mux/demux should permit the frequency range of operation to be easily tuned. Here we propose an approach based on a waveguide-based inhomogeneous medium, which can satisfy these requirements. Previously, a proposed 3D printed tunable prism capable of separating the frequency components of a broadband pulse was proposed. Due to fabrication limitations, the device is only able to work for frequencies below 500 GHz [17]. The device proposed in this Letter has the capability to operate for frequencies between 0.2 and 1 THz.

Our device is based on a stack of seven stainless-steel sheets of different lengths, as shown in Fig. 1. The length of every plate (along the z direction) changes in a linear fashion, ranging from 4 mm at the top to 10 mm at the bottom, in steps of 1 mm. The thickness of each metallic sheet is 0.1 mm, which is sufficient to provide mechanical stability, while the width (x direction) is 2 cm. The height of the entire array (y direction) is 6 (when the spacing between adjacent plates is 0.8 mm) or 4.5 mm (when the plate spacing is 0.55 mm). Therefore, the stack of plates therefore has two effective surfaces, one (on the input side) which is normal to the nominal propagation direction of the incoming radiation and a second (at the output) which is not. An incident wave, polarized parallel to the plate surfaces, excites a series of transverse-electric modes in the gaps between the adjacent plates (dominantly, the TE_1 mode) [18,19]. Conversely, if the input polarization is perpendicular to the plate surfaces, the TEM modes are excited. At the exit face, due to the mode-dependent impedance mismatch between the parallel-plate waveguide (PPWG) structure and the surrounding medium (air), the THz radiation is deflected. Because this impedance mismatch is frequency dependent, each frequency component is deflected at a unique angle. The numerical results are shown in Figs. 1(b) and 1(c), validating this demux functionality. The frequency range of operation is fixed by the separation of the metallic plates, with the lower limit given by the cutoff frequency and the upper limit determined by when the impedance mismatch

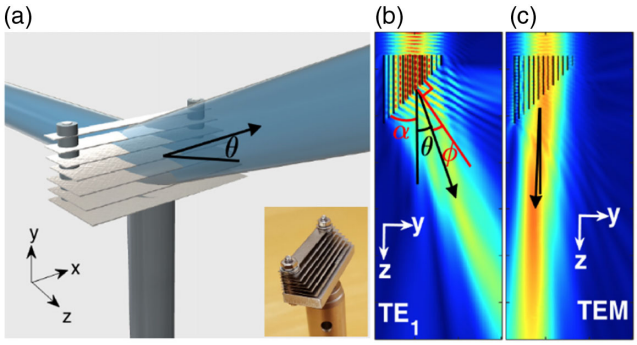

Fig. 1. (a) Schematic diagram of the proposed demultiplexer. The incoming beam impinges on the back surface of the demultiplexer forming guided modes inside the structure. The exit beam is deflected by an angle θ which depends on the frequency of the signal and on the dimensions of the structure. The inset shows a photograph of the device. (b)–(c) Finite-element simulation at 0.3 THz when the spacing between plates is 0.8 mm for the TE_1 and TEM guided-modes, respectively.

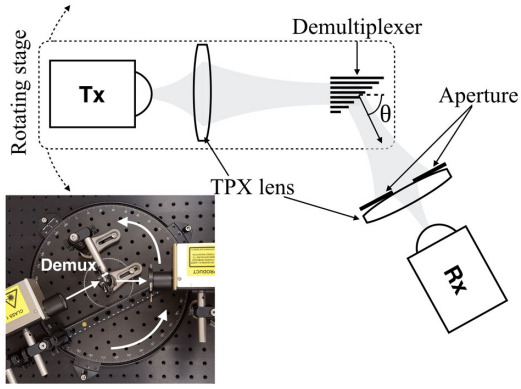

Fig. 2. Experimental setup. The transmitter and the demultiplexer were fixed on a rotating stage, while the receiver (Rx) was fixed on the optical table. An aperture of 2.5 mm was used in front of the receiver in order to improve the spatial resolution. Inset: photograph of the experimental setup.

becomes negligible, or when significant multi-mode excitation becomes unavoidable. The numerical simulations were carried out using COMSOL multiphysics. For the TE_1 mode, the frequency-dependent impedance is given by [20]

$$Z_{\mathrm{TE}} = \frac{k_0\eta_0}{k_{\mathrm{PPWG}}} = \frac{\eta_0}{\sqrt{\left(1-\frac{c^2}{4h^2f^2}\right)}}, \tag{1}$$

where k_0 is the propagation constant in free space, k_{PPWG} is the propagation constant inside the PPWG, η_0 is the free space impedance, c the speed of light in vacuum, h is the spacing between plates, and f is the frequency. Meanwhile, the TEM mode is characterized by its non-dispersive behavior (i.e., $k_0 = k_{\mathrm{PPWG}}$) [18]. Thus, if the dielectric medium filling the waveguide is the same as the surrounding medium, then there is no impedance mismatch, and the beam is not deflected at any frequency [Fig. 1(c)]. In contrast, the TE mode is significantly deflected [Fig. 1(b)]. Because of the aforementioned characteristics, the demultiplexer shown in Fig. 1 presents two different mechanisms for splitting a signal, based on either polarization (TE_1 and TEM) or frequency (TE_1 only). To predict the deflected angle of the THz beam, we first consider the boundary conditions at the exit face of the demultiplexer:

$$k_0 \sin(\varphi) = k^{\parallel}_{\mathrm{PPWG}}. \tag{2}$$

From Fig. 1(a), the projection of k_{PPWG} parallel to the exit face is

$$k^{\parallel}_{\mathrm{PPWG}} = k_{\mathrm{PPWG}} \cos\left(\tan^{-1}(h/b)\right). \tag{3}$$

Substituting Eq. (3) into Eq. (2) and reordering,

$$\varphi = \sin^{-1}\left(\cos\left(\tan^{-1}\left(\frac{h}{b}\right)\right)\sqrt{1-\frac{c^2}{4h^2f^2}}\right). \tag{4}$$

Furthermore, from Fig. 1, the relation between φ and θ is

$$\theta + \varphi + \alpha = \frac{\pi}{2}, \tag{5}$$

where $\alpha = \tan^{-1}(h/b)$. Substituting Eq. (4) and α in Eq. (5),

$$\theta = \frac{\pi}{2} - \tan^{-1}\left(\frac{h}{b}\right) - \sin^{-1}\left(\cos\left(\tan^{-1}\left(\frac{h}{b}\right)\right)\sqrt{1-\frac{f_c^2}{f^2}}\right) \tag{6}$$

is the theoretical deflection angle as a function of frequency for the TE mode, where $f_c = c/2h$.

To characterize the proposed demultiplexer, we use the Terapulse 4000 THz-TDS spectrometer from TeraView Ltd. with a spectral resolution of 4.5 GHz in the configuration shown in Fig. 2. This setup allows for the angle variation between the exit face of the demultiplexer and the receiver. An aperture size of 2.5 mm is placed in front of the receiver in order to improve the spatial resolution. In this Letter, we study two demultiplexers with two different values of the plate spacing in order to highlight the tunability of the device. In Fig. 3, the experimental results for the two demultiplexers are presented for both TE_1 and TEM modes. These results have been normalized to the THz beam propagated through free space.

Figures 3(a) and 3(b) show the experimental deflected angle for the electric field of the TE_1 and TEM components for the 0.55 mm spaced demultiplexer. The detection angle was changed from 0° to 40° in steps of 2° for a frequency range from 0.18 to 1 THz. Figures 3(c) and 3(d) show the deflected angle for the two orthogonal components (TE_1 and TEM) for the 0.8 mm spaced device. This time the exit angle was changed from 0° to 24° in steps of 1°. The dashed black lines in Figs. 3(a) and 3(c) are the predictions from Eq. (6); the dashed red lines indicate the waveguide cutoff frequency given by $f_c = c/2h$ [21]. The experimental results are in excellent agreement with the theory and indicate how the deflected angle can be increased to 40° by simply reducing the spacing between plates from 0.8 to 0.55 mm for the same frequency range. In contrast, from Figs. 3(b) and 3(d), as expected, the TEM components present no deflection after propagation through the demultiplexer since TEM modes are not dispersive [20], and they have the same effective refractive index as the surrounding medium (air). For this reason, this technology is able to effectively separate the two orthogonal polarization components. The color maps in the

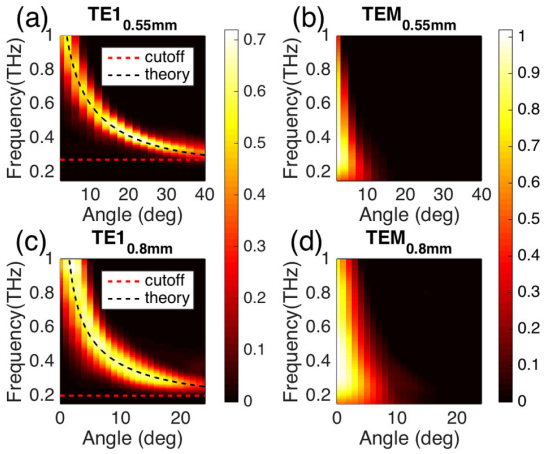

Fig. 3. Experimental E-field transmission amplitude. (a) and (b) show the deflected angle electric field of the TE_1 and TEM modes for the 0.55 mm spaced demultiplexer. (c) and (d) present similar results, but this time for the 0.8 mm spaced demultiplexer. In (a) and (c), the dashed black lines represent the predicted deflected angle given by Eq. (6); meanwhile, the dashed red lines represent the cutoff frequency.

figures show the electric field amplitude transmitted through the device and indicate a maximum amplitude transmission of around 70% which corresponds to insertion losses of 3.1 dB in the intensity transmission coefficient for the TE_1 mode. These values include the impedance mismatch losses between the impedance of the structure and the surrounding, as well as to ohmic losses and higher-mode coupling losses, which limits the performance of the device for higher frequencies. Nevertheless, it is clear that the excitation of higher-order modes is only a relatively small effect, since no other cutoff frequencies are observed in Fig. 3. The effective operating bandwidth of the device approaches 1 THz, which is several times larger than the TE_1 mode cutoff frequency. In Fig. 4, we show the normalized theoretical attenuation due to ohmic losses for the different waveguide excited modes [20]. Given that the electric field's amplitude does not vary across any waveguide's aperture, even-order TE modes (TE_2, TM_2, ...) are not excited. From the curves, it is clear that the lowest TE mode and the TEM mode are the least attenuated modes within the frequency range of operation. This ensures that any residual excitation of higher modes will have minimal effect on the output (other than increasing the overall insertion loss), as these modes are rapidly extinguished within the demultiplexer.

Another important performance metric for the proposed demultiplexer is the channel bandwidth, i.e., the range of frequencies detected for a given detection configuration. The bandwidth can be calculated by taking the derivative of Eq. (2) [22]:

$$\Delta f = \frac{\Delta\theta}{\left|\frac{d\theta}{df}\right|} = \frac{\Delta\theta c f\sqrt{1-\frac{f_c^2}{f^2}}}{2haf_c^2}, \tag{7}$$

where θ is given by Eq. (2), $a = \cos(\tan^{-1}(h/b))$, and fc is the cutoff frequency. The acceptance angle, $\Delta\theta$ in Eq. (7), depends

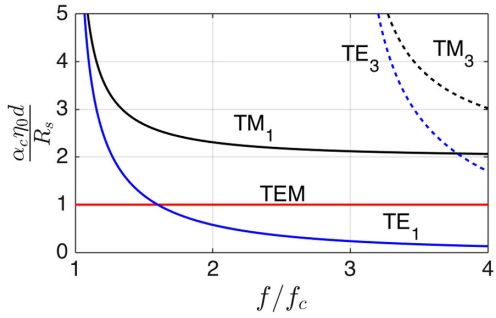

Fig. 4. Normalized ohmic losses for the TE and TM modes. α_c is the ohmic loss coefficient, η_0 is the vacuum impedance, d is the spacing b between plates, and R_s is the surface resistivity of stainless steel [20]. In this figure, it can be seen that the TE_1 and the TEM modes have the lowest ohmic loss coefficients, while the higher-order modes have a normalized absorption coefficient greater than two within the operational frequency.

on the aperture and the focal length of the lenses used. The aperture is shown in Fig. 2 and has a value of 2.5 mm in our measurements. In this case, we find $\Delta\theta = 0.018°$. To obtain the experimental bandwidth from Figs. 3(a) and 3(c), a Gaussian curve has been fitted for every deflected angle along the frequency axis (y axis). Using the fitted Gaussian curve, the 3 dB bandwidth can be extracted [22]. The results are shown in Fig. 5(a).

As seen in Eq. (7), the bandwidth depends on the aperture used for detection. Ideally, with an infinitesimally small aperture, this formalism suggests that arbitrarily narrow bands could be measured at unique angles. This is experimentally impossible, of course, if for no other reason than the spectral intensity per unit bandwidth is finite (in fact, quite low) in our THz time-domain measurements. However, we note that the channel bandwidth can be controlled at least over some range by selecting the appropriate size for the detector acceptance aperture. In Fig. 5(b), we plot the detected time-domain THz electric field for the 0.8 mm demultiplexer at different detector angles. It is clear that the duration of the THz wave becomes more extended as the exit angle increases, as expected from Fig. 5(a).

To explore another functionality of this device design, we add a second demultiplexer next to the first one, forming the triangular structure shown in Fig. 6.

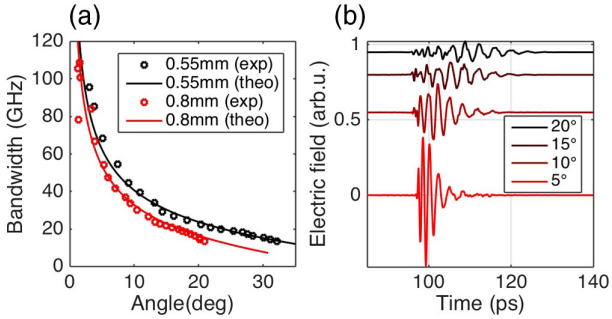

Fig. 5. (a) Bandwidth characterization for the 0.55 and 0.8 mm demultiplexer. The solid lines indicate the theoretical prediction by Eq. (7), and the dots indicate the 3 dB bandwidth. (b) Electric field time trace of the deflected THz wave at 5°, 10°, 15°, and 20° for the 0.8 mm spaced demultiplexer. The THz traces have been offset in the vertical direction for clarity.

In this new configuration, the demultiplexer forms a fifty-fifty amplitude splitter for the TE_1 mode. This result is demonstrated in Fig. 6(a) for the case of 0.55 mm plate spacing. The black dashed lines in Fig. 6(a) indicate the theoretical results obtained using Eq. (6). The idea of amplitude splitters using PPWGs has been explored previously using different geometries [23,24]. Here we note that our triangular geometry provides beam splitting without the need to change the incident angle or operate any movable parts. From the experimental results, an equal transmission splitting is obtained for frequencies between 0.2 and 1 THz. In Fig. 6(b), we observe experimental transmission results for the TEM component that are slightly higher than unity. This is the result of a small focusing effect at lower frequencies due to edge diffraction from the abruptly terminated metal plates. Indeed, the same edge diffraction effect is also observed in Fig. 1(c) (see the black arrow, which is slightly deflected relative to the input normal). Not surprisingly, these edge effects are stronger at lower frequencies, resulting in higher values for the transmission at lower frequencies. The beam transmitted after the device keeps its Gaussian profile for the TM components due to the weak interaction with the splitter. However, for the TE modes, the exit beam profile does not present a Gaussian profile due the strong interaction with the device. This is confirmed by the simulation in Fig. 1(b). The Gaussian profile could be fixed using additional optics if desired, depending on the specific application.

In conclusion, we demonstrate a novel device concept for the demultiplexing of THz radiation based on PPWG technology. Due to the artificial birefringence presented in PPWGs, our device is able to split the two orthogonal polarization states (vertical and horizontal) with angles higher than 40°. Additionally, given the unique dispersive properties of these waveguides, a highly sensitive polarization demux is also reported. With the addition of a second demultiplexer, we finally demonstrate a fifty-fifty amplitude splitter. This is the first demonstration of a combined frequency/polarization and amplitude splitter using PPWG technology for the 0.2 to 1 THz range in the same device. Given the versatility of PPWG structures, the frequency range of operation of the splitter can be easily tuned only by changing the spacing between plates, contrasting with typical splitters fixed at specific frequency bands. As future work, we envisage a tunable demultiplexer capable of actively controlling the deflected exit angle and the frequency range of operation. This splitter represents an inexpensive, mechanically robust, and versatile approach for the next generation of communication devices for THz wireless networks.

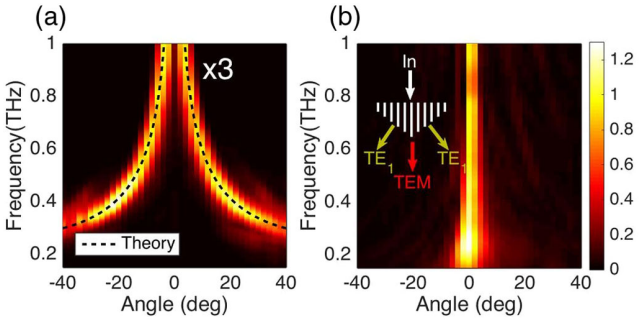

Fig. 6. Experimental results for the fifty-fifty amplitude splitter with 0.55 mm spacing. (a) Transmission of the TE_1 component shows an equal amplitude separation with exit angles between −40° to 40°. The black dashed lines indicate the theoretical deflected angle using Eq. (6). (b) Transmission for the TEM components. The transmission values above 1 are observed for frequencies close to 0.2 THz due to the strong edge effects at these frequencies which slightly deflect the outgoing radiation towards the center of the demultiplexer focusing the energy. In (a), the transmission of the TE_1 mode has been multiplied by a factor of three to match with the color scale in (b).

Funding. Engineering and Physical Sciences Research Council (EP/S021442/1); National Science Foundation; Royal Society (Wolfson Merit Award).

Acknowledgment. The authors thank the Optics Laboratory at Warwick University for the use of their equipment. The datasets used in this work are available from https://figshare.com/articles/Data_demux_zip/11627379.

Disclosures. The authors declare no conflicts of interest.

REFERENCES

1. T. Kleine-Ostmann and T. Nagatsuma, J. Infrared, Millimeter, Terahertz Waves **32**, 143 (2011).
2. R. Piesiewicz, T. Kleine-Ostmann, N. Krumbholz, D. Mittleman, M. Koch, J. Schoebei, and T. Kurner, IEEE Antennas Propag. Mag. **49**, 24 (2007).
3. K. Sengupta, T. Nagatsuma, and D. M. Mittleman, Nat. Electron. **1**, 622 (2018).
4. Y. Monnai, K. Altmann, C. Jansen, H. Hillmer, M. Koch, and H. Shinoda, Opt. Express **21**, 2347 (2013).
5. H.-J. Song, K. Ajito, Y. Muramoto, A. Wakatsuki, T. Nagatsuma, and N. Kukutsu, Electron. Lett. **48**, 953 (2012).
6. Z. Chen, X. Chen, L. Tao, K. Chen, M. Long, X. Liu, K. Yan, R. I. Stantchev, E. Pickwell-MacPherson, and J.-B. Xu, Nat. Commun. **9**, 1 (2018).
7. D. Headland, Y. Monnai, D. Abbott, C. Fumeaux, and W. Withayachumnankul, APL Photonics **3**, 051101 (2018).
8. M. Yata, M. Fujita, and T. Nagatsuma, Opt. Express **24**, 7835 (2016).
9. J. Ma, M. Weidenbach, R. Guo, M. Koch, and D. Mittleman, J. Infrared Millimeter, Terahertz Waves **38**, 1316 (2017).
10. S. Koenig, D. Lopez-Diaz, J. Antes, F. Boes, R. Henneberger, A. Leuther, A. Tessmann, R. Schmogrow, D. Hillerkuss, R. Palmer, and T. Zwick, Nat. Photonics **7**, 977 (2013).
11. H.-J. Song, J.-Y. Kim, K. Ajito, N. Kukutsu, and M. Yaita, IEEE Trans. Microw. Theory Tech. **62**, 600 (2014).
12. T. Nagatsuma, G. Ducournau, and C. C. Renaud, Nat. Photonics **10**, 371 (2016).
13. S. Cherry, IEEE Spectrum **41**, 58 (2004).
14. J. Y. Suen, M. T. Fang, and P. M. Lubin, IEEE Trans. Terahertz Sci. Technol. **4**, 86 (2014).
15. Y. Yang, M. Mandehgar, and D. Grischkowsky, Opt. Express **22**, 4388 (2014).
16. K. Su, L. Moeller, R. B. Barat, and J. F. Federici, J. Opt. Soc. Am. A **29**, 2360 (2012).
17. S. F. Busch, E. Castro-Camus, F. Beltran-Mejia, J. C. Balzer, and M. Koch, J. Infrared Millimeter, Terahertz Waves **39**, 553 (2018).
18. R. Mendis and D. M. Mittleman, J. Opt. Soc. Am. B **26**, A6 (2009).
19. A. Hernandez-Serrano, R. Mendis, K. S. Reichel, W. Zhang, E. Castro-Camus, and D. M. Mittleman, Opt. Express **26**, 3702 (2018).
20. D. M. Pozar, *Microwave Engineering* (Wiley, 2009).
21. A. Hernandez-Serrano, Q. Sun, E. G. Bishop, E. R. Griffiths, C. P. Purssell, S. J. Leigh, J. Lloyd-Hughes, and E. Pickwell-MacPherson, Opt. Express **27**, 11635 (2019).
22. N. J. Karl, R. W. McKinney, Y. Monnai, R. Mendis, and D. M. Mittleman, Nat. Photonics **9**, 717 (2015).
23. R. Mendis, M. Nagai, W. Zhang, and D. M. Mittleman, Sci. Rep. **7**, 5909 (2017).
24. K. S. Reichel, R. Mendis, and D. M. Mittleman, Sci. Rep. **6**, 28925 (2016).